# Bulk to nanoscale magnetism and exchange bias in CuO nanoparticles

A. Punnoose, H. Magnone, and M. S. Seehra*
*Department of Physics, West Virginia University, Morgantown, West Virginia 26506-6315*

J. Bonevich
*National Institute of Standards and Technology, Gaithersburg, Maryland 20899-8562*
(Received 28 June 2001; published 15 October 2001)

Detailed studies of the temperature (5–350 K) and magnetic field variations (up to $H=50$ kOe) of the magnetization of CuO nanoparticles of nominal size range 37–6.6 nm are reported. These particles were synthesized by the sol-gel method in combination with high-temperature annealing, followed by structural characterization by x-ray diffraction and high-resolution transmission electron microscopy. With a decrease in particle size $d$ from 37 to 10 nm, the unit-cell volume and $b$ axis increased and the bulk Néel temperature $T_N$ decreased according to $\gamma_m = -\partial \ln T_N / \partial \ln b = 30$. For particles with $d<10$ nm, there is a more rapid lattice expansion and the magnetic susceptibility $\chi$ varied as $1/d$, accompanied by a weak ferromagnetic component and hysteresis loops. For the 6.6-nm particles for which detailed studies are reported, there is a rapid increase in the coercivity $H_c$ and the remanence $M_r$ below 40 K accompanied by an exchange bias $H_E$ for the field-cooled samples in $H=50$ kOe. From 10 to 40 K, $H_E$ decreases monotonically to zero. However, above 40 K, a symmetric hysteresis loop is observed, with $H_c$ decreasing weakly towards zero as temperature increases towards 330 K. The hysteresis loop and the $1/d$ variation of $\chi$ are interpreted in terms of uncompensated surface $Cu^{2+}$ spins, whereas the transition at 40 K is suggested to be $T_N$ of the spins in the core of 6.6-nm particles. Similarities to the hysteresis loops observed in the Permalloy/CoO system are noted.

DOI: 10.1103/PhysRevB.64.174420 PACS number(s): 75.50.Tt, 75.30.Kz, 75.30.Cr, 81.07.−b

## I. INTRODUCTION

The nature of magnetism in nanoscale particles (NP's) has become a very active area of research because of the unique properties of NP's and their potential technological applications.[1–3] In NP's with an antiferromagnetically ordered core, the surface spins are expected to dominate the measured magnetization because of their lower coordination and uncompensated exchange couplings.[3,4] This in turn leads to a large magnetic moment per particle and modified superparamagnetism.[5–7] Considerable variations of the magnetic properties with change in particle sizes are expected because of the associated changes in the relative number of surface spins. Antiferromagnetic NP systems where detailed magnetic studies have been reported include NiO,[3,6] ferritin,[5,8] $\alpha$-$Fe_2O_3$,[9,10] and ferrihydrites.[7,11]

The transition-metal monoxides MnO, FeO, CoO, NiO, and CuO are all antiferromagnets. Whereas MnO, FeO, CoO, and NiO crystallize in the NaCl structure, CuO is unique in having a monoclinic unit cell and square-planer coordination of copper by oxygen.[12] Because of the similarity of this coordination of Cu to that in high-$T_c$ superconductors, bulk CuO has been investigated by a variety of experimental techniques in recent years. From the temperature variations of the magnetic susceptibility $\chi$,[13–15] specific heat,[14,16,17] and neutron diffraction[18] in bulk CuO, it is well established that a transition from a paramagnetic to incommensurate antiferromagnetic (AF) state occurs near $T_N \simeq 230$ K, followed by a first-order transition to commensurate AF state near 213 K, with the moments aligned along the monoclinic $b$ axis. In addition, the continued rise in $\chi$ above $T_N$, with a broad maximum occurring near 550 K, has been explained in terms of linear chain antiferromagnetism, with intrachain exchange constant $J \simeq 400$ K.[19] These Cu-O-Cu chains are evident in the crystal structure along $[1\,0\,\bar{1}]$, with a Cu-O-Cu bond angle of 146°. The rise in $\chi$ observed for $T<140$ K in many studies can be attributed to defects or impurities[13,14,20] since in high-purity single crystals, this rise in $\chi$ at lower temperatures is not observed.[15,21]

In this paper, we report the synthesis of CuO NP's in the 37–6.6 nm range by the sol-gel route and high temperature annealing, followed by structural characterization using x-ray diffraction and transmission electron microscopy and detailed magnetic studies in the 5–350 K range and in magnetic fields up to 50 kOe. Whereas the magnetic behavior of the particles with size $d \geqslant 10$ nm resembles that of bulk CuO except for reduced $T_N$ due to expansion of the lattice, particles with size $d<10$ nm exhibit anomalous magnetic properties and hysteresis loops. For the 6.6-nm particles for which detailed studies are reported, a $T_N \simeq 40$ K is inferred below which significant exchange bias $H_E$ with enhanced coercivity $H_c$ is observed for the field-cooled (FC) sample. From 40 to 330 K a symmetric hysteresis loop is observed with slowly decreasing $H_c$ with increase in temperature. Details of these results and their interpretation are presented below.

## II. EXPERIMENTAL DETAILS

CuO NP's were prepared by the sol-gel method by reacting at room temperature acquous solutions of copper nitrate and sodium hydroxide at $p\mathrm{H}=10$. The resulting gel was washed several times with distilled water until free of nitrate ions. This gel was then centrifuged and dried in air. The resulting sample, analyzed by x-ray diffraction (XRD) using a Rigaku diffractometer and CuK$\alpha$ radiation ($\lambda$

 

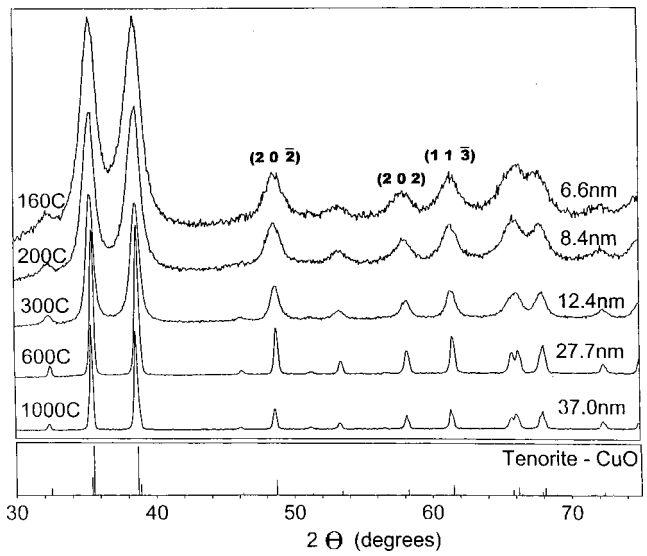


FIG. 1. Room-temperature XRD patterns of CuO particles annealed at different temperatures shown. The particle size shown is the average value determined from the $(20\bar{2})$, (202), and $(11\bar{3})$ lines using the Scherrer relation, after correcting for the instrumental width (e.g., see Ref. 10). Temperatures are in °C.

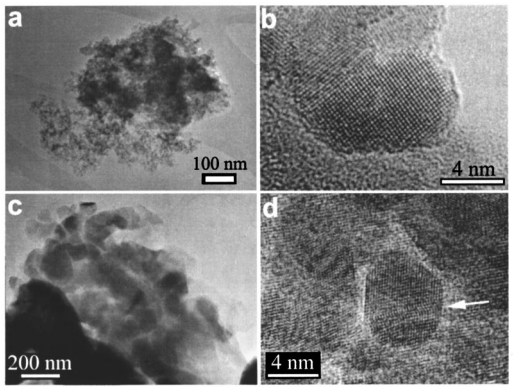


FIG. 2. TEM characterization reveals agglomeration of the nanoscale particles. A cluster of 6.6-nm particles, shown in (a), consists of highly faceted single particles (b). A cluster of the nominal 33-nm particles is shown in (c). These large particles have surfaces decorated with smaller particles (d), which exhibit defects such as multiple twinning (arrow).

$=0.15418$ nm) was found to be pure $Cu(OH)_2$. Thermogravimetric measurements, carried out in air using a Mettler TA3000 system, showed that $Cu(OH)_2$ dissociates into CuO near 160 °C. Consequently, the $Cu(OH)_2$ gel was calcined in air for 3 h at the selected temperatures of 160, 200, 250, 300, 400, 600, 800, and 1000 °C. The XRD patterns of the calcined samples (Fig. 1) show only lines due to CuO. Employing the Scherrer relation with instrumental correction,[10] the average particle sizes determined from the $(20\bar{2})$, (202), and $(11\bar{3})$ reflections are listed in Fig. 1. The above procedure for synthesis, somewhat similar to the one used for producing NiO NP's,[6] differs substantially from the electrochemical technique used recently by Borgohain *et al.* where encapsulated CuO NP's of 3–6 nm size were produced.[22] The fact that in Fig. 1 no phase other than CuO (e.g., $Cu_2O$) is detected is important since a recent report by Palkar *et al.*[23] states that CuO NP's below 25 nm are not stable and convert to $Cu_2O$. However, the method used by Palkar *et al.* for synthesis was different involving citrates and oxalates.

The above-prepared samples were characterized at the National Institute of Standards and Technology by x-ray energy dispersive spectroscopy to verify that particles are indeed CuO and by HRTEM to verify the particle size and morphology. In Fig. 2, we show selected TEM micrographs. In addition to the expected fusion of the particles with sintering, surface facetting is evident. The small particles are aggregated and the size of the smaller particles as measured by TEM is comparable to the numbers determined from the XRD patterns. However, for larger particles of nominal sizes $\geqslant 27.7$ nm, there are differences in the sizes observed in TEM, which indicates considerably larger sizes and the presence of smaller particles on the surface of the larger particles, suggesting a bimodal distribution [Fig. 2(d)]. This discrepancy is most likely due to the inadequacy of the Scherrer relation to yield accurate results for larger particles where the linewidths become comparable to the instrumental width. This discrepancy, however, has no significant bearing on the results presented here since the magnetic properties of these larger particles resemble those of bulk CuO anyway. The new interesting properties are observed for sizes $\leqslant 10$ nm for which there is a good agreement between the sizes determined from XRD and TEM measurements.

The temperature and magnetic field variations of the magnetization $M$ for all our samples were measured with a superconducting quantum interference device (SQUID) magnetometer. For the zero-field-cooled (ZFC) case, the samples were cooled to 5 K in zero field, a measuring field was then applied, followed by data acquisition at increasing temperatures by stabilizing the temperature at each point. For the FC case, the sample was cooled in a specified $H$ to 5 K, followed by data acquisition in the above manner. For some specified cases, the FC data were taken with decreasing temperatures. The measured $M$ values are corrected for the weak diamagnetic contribution of the white plastic drinking straw used as a sample holder, as described in Ref. 7.

## III. EXPERIMENTAL RESULTS AND DISCUSSION

### A. Lattice parameters

The lattice parameters $a$, $b$, $c$, and $\beta$ of the monoclinic unit cell of CuO were determined from the XRD patterns of Fig. 1 using the Jade pattern analysis software. The largest change with particle size was observed for the $b$ axis. Consequently, we show in Fig. 3 the variation of the $b$ axis and the unit-cell volume $V=abc\sin\beta$ with particle size, both of which increase as particle size decreases, with a large increase in the rate occurring for particles below 10 nm. In a recent paper, Ayyub *et al.*[24] have argued that such lattice expansion and distortion can occur with a reduction in particle size. Since Cu-O-Cu superexchange is expected to be a strong function of both the bond angle and bond length, no-

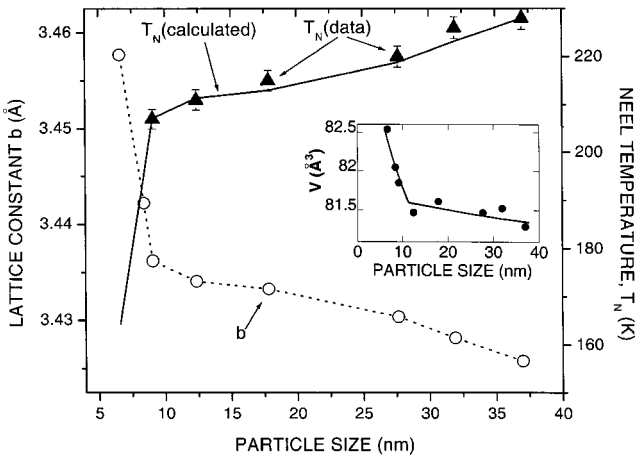


FIG. 3. Size dependence of the lattice constant of $b$ axis, the volume of the unit cell (inset), and the measured Néel temperature $T_N$. The solid line is drawn using $\gamma_m = -\partial \ln T_N / \partial \ln b = 30$. The dotted line is drawn connecting the points.

ticeable changes in the magnetic properties should be expected with reduction in particle size. This is indeed observed as described below.

### B. Magnetic susceptibility and Néel temperature

The temperature variation of magnetic susceptibility $\chi = M/H (H = 200\,\text{Oe})$ for the ZFC cases is plotted in Fig. 4

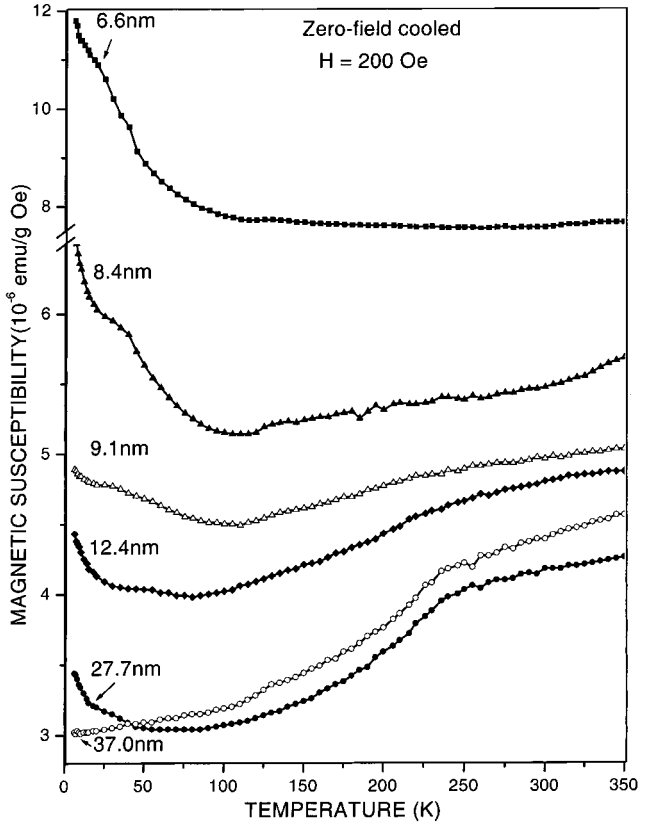


FIG. 4. Temperature variation of the magnetic susceptibility $\chi$ for different particles indicated.

for particle sizes of 6.6, 8.4, 9.1, 12.4, 27.7, and 37 nm.[25] For the larger particles, the data are similar to the observation in bulk CuO.[13–15] The Néel temperature $T_N$ for the largest 37-nm particle determined by locating the peak in $\partial(\chi T)/\partial T$ versus $T$ (Ref. 26) yields $T_N \simeq 228\,\text{K}$, in close agreement with the known $T_N \simeq 230\,\text{K}$ for bulk CuO. Above $T_N$, $\chi$ in CuO continues to rise due to one-dimensional short-range order, in agreement with earlier observations in bulk CuO.[13] For particles down to 9.1 nm, $T_N$ could be determined in a similar fashion from the peak in $\partial(\chi T)/\partial T$ and these values of $T_N$ (shown as solid triangles with error bars indicating experimental uncertainty) versus particle size are also plotted in Fig. 3. The small rise in $\chi$ seen at low temperatures for the larger particles may be due to the already noted small particle inclusions in larger particles, as observed in HRTEM (Fig. 2). For the 6.6 and 8.4-nm particles, no peak in $\partial(\chi T)/\partial T$ was evident.

The changes in $T_N$ and the lattice constant $b$ with particle size (Fig. 3) may be interpreted in terms of the magnetic Gruneisen parameter $\gamma_m \equiv -\partial \ln T_N / \partial \ln b$ since the expansion of the lattice is expected to decrease exchange constants and hence $T_N$. The solid line shown in Fig. 3 corresponds to $\gamma_m = 30$. In bulk antiferromagnets with superexchange interactions, $\gamma_m \simeq 10$ is usually found assuming $T_N \propto J$.[27] In CuO, $T_N$ is most likely triggered by the weaker interchain exchange interaction. Consequently, the larger value of $\gamma_m$ observed here may reflect this complication and possible contributions from the finite-size effects.[27] If the same $\gamma_m = 30$ is assumed for the 6.6-nm particles, $T_N \simeq 170\,\text{K}$ should have been observed for these particles (Fig. 3).

Comparison of the behavior of $\chi$ vs. $T$ for the largest (37 nm) and the smallest (6.6 nm) particles in our study is made in Fig. 5 where data for both the FC and ZFC cases in $H = 200\,\text{Oe}$ are presented. The difference susceptibility $[\chi(\text{FC}) - \chi(\text{ZFC})]$ for the two cases, plotted in the inset of Fig. 5 as a function of temperature, clearly brings out the different nature of magnetism in the 6.6-nm particles, as indicated by the anomaly near 40 K. The nature of this anomaly is investigated in more detail later.

### C. Magnetization versus magnetic field variations

The plots of $M$ versus $H$ at different temperatures between 5 and 300 K are shown in Fig. 6 for the 6.6- and 32-nm particles. The plots are essentially linear up to 50 kOe except for a weak ferromagnetic (WF) component at lower fields. The magnitude of the WF component is much larger in the 6.6-nm particles as evident from the plot of $M$ versus $H$ for lower fields (Fig. 7). Following the TEM observations of inclusion of some smaller particles in larger particles, we infer that the WF component in larger particles originates from particles smaller than 10 nm only. The variation of $M$ versus $H$ in Fig. 7 even for the 6.6-nm particles is quite different from the Langevin-type variation observed in AF NP's of ferritin[5] and ferrihydrite.[7] The WF component appears to saturate at $H \simeq 3\,\text{kOe}$, and its magnitude extrapolated to $H = 0$ equals 0.008 emu/g for the 6.6-nm particles. As a comparison, for the 5.3-nm NiO particles with $T_B \simeq 160\,\text{K}$, $M \simeq 2$ emu/g for $H \to 0$ Oe was observed, suggest-

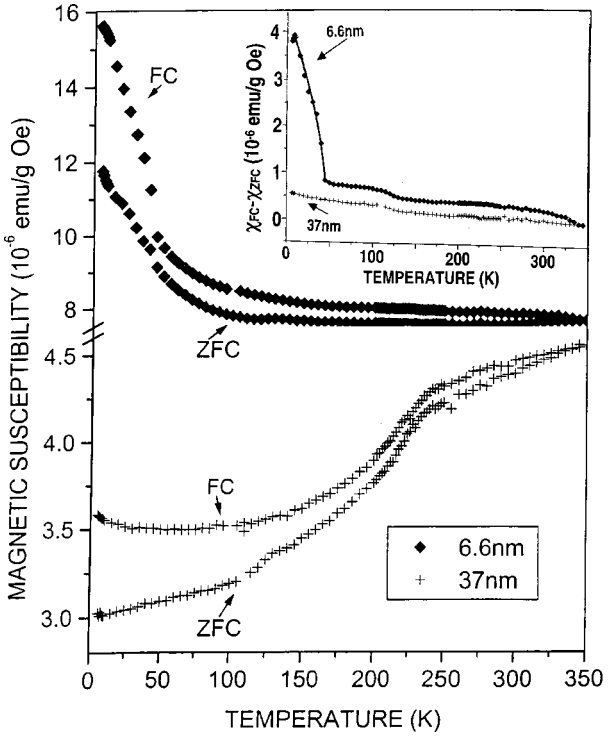


FIG. 5. Temperature variations of the magnetic susceptibility $\chi$ under ZFC (zero-field-cooled) and FC (field-cooled) conditions for the largest (37 nm) and the smallest (6.6 nm) particles. In the inset, the difference susceptibility $[\chi(\mathrm{FC})-\chi(\mathrm{ZFC})]$ is plotted against temperature for the largest (37 nm) and the smallest (6.6 nm) particles. The lines joining the points are for visual aid.

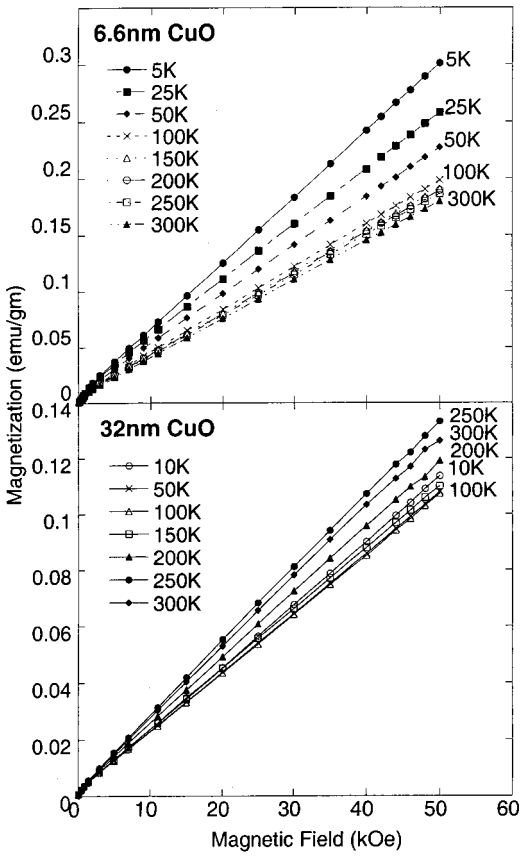


FIG. 6. Measured magnetization $M$ of the 6.6- and 32-nm particles as a function of applied field $H$ up to 50 kOe at selected temperatures between 5 and 300 K. Lines joining the points are for visual aid.

ing that the nature of surface spin disorder in CuO NP's is quite different from the observations in other well-studied AF-NP systems such as ferritin,[5] NiO,[6] and ferrihydrite.[7] Even for NiO NP's, the $M$ vs $H$ variation could not be fitted to the Langevin-type variation observed in ferritin[5] and ferrihydrite[7] NP's with a realistic value of the particle moment. This is even more valid for the CuO-NP system described here.

### D. Particle-size dependence of magnetic susceptibility

Richardson *et al.*[28] have discussed the various cases of the Néel's model for the uncompensated spins $p=n_A-n_B$, where $n_A$ and $n_B$ are the number of atoms on a two-sublattice antiferromagnet. The magnetic moment for $H\rightarrow 0$ depends on $p$, which in turn depends on the crystal structure, particle morphology, and particle size. For a particle of size $d$, the number $n$ of atoms per particle with magnetic moment $\mu_a$ on each and interatomic distance of $a$ is given by $n=d^3/a^3$. The mass susceptibility $\chi$ for particles of density $\rho$ is then given by

$$\chi=\chi_T+\frac{\mu_a^2\mu_B^2}{\rho a^3(3k_BT)}\left(\frac{p^2}{n}\right), \qquad (1)$$

where $\chi_T$ is the susceptibility of the compensated system, $k_B$=Boltzmann's constant, and $\mu_B$=Bohr magneton. The dependence of $p$ on $n$ and hence $d$ goes as follows: (i) $p=n^{1/2}$ for random distribution of missing $B$ spins, (ii) $p=n^{2/3}$ if the top and bottom layers of a particle belong to the same sublattice, and (iii) $p=n^{1/3}$ if only the alternating planes belonging to the same sublattice of the top and bottom layers are uncompensated. For $p=n^{1/2}$, $p^2/n$ in Eq. (1) is constant and independent of $d$; for $p=n^{2/3}$, $p^2/n=n^{1/3}=d/a$; and for $p=n^{1/3}$, $p^2/n=1/n^{1/3}=a/d$. Thus the $d$ dependence of $\chi$ is different from the three cases.

To check the $d$ dependence of $\chi$, we plot in Fig. 8, $\chi$ versus $1/d$ since our observations suggest that $\chi$ goes up as $d$ decreases. Data for particles with $d<10$ nm clearly follow the linear dependence expected for the case (iii) with $p=n^{1/3}$. Although the expected increase in $\chi$ with decrease in temperature [Eq. (1)] is observed, the $1/T$ dependence is not strictly obeyed, as was obvious from Fig. 4 also. The $1/d$ dependence of Fig. 8 is similar to the observation in NiO NP's,[28] but different from the observations in ferritin[5] and ferrihydrite[7] NP's where the experimental observations fitted the $p=n^{1/2}$ variation. The magnetic moment $\mu_a$ calculated from the slope of Fig. 8 and Eq. (1) for the 6.6-nm particles equals $0.16\mu_B$ at 7 K and $0.72\mu_B$ at 350 K. The magnetic moment per Cu atom measured by neutron diffraction is $0.65\mu_B$ in CuO,[18] in agreement with our higher-temperature estimate.

From the above results, it is concluded that in CuO-NP

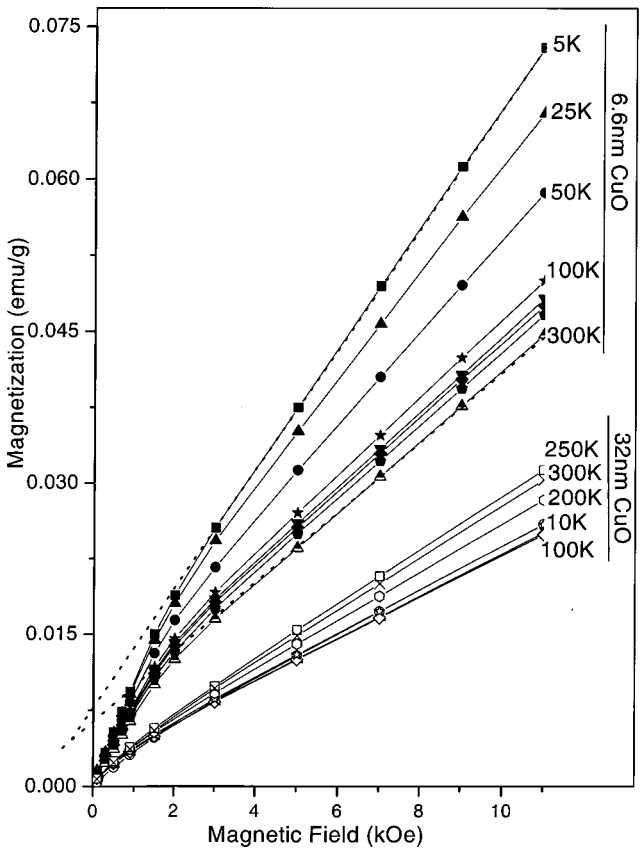


FIG. 7. Expansion of the data of Fig. 6 for lower fields to show the weak ferromagnetic component which saturates at about 3 kOe.

systems, particles with $d>10$ nm behave essentially as bulk CuO except for the lowered $T_N$ due to the expansion of the lattice. However, for particles with $d<10$ nm, nanomagnetism comes into play since the expected $T_N=170$ K for the 6.6-nm particles is not observed. Also, $1/d$ variation of $\chi$ and the resulting calculated magnetic moment $\mu_a$/Cu atom are consistent with the case of Néel's model in which alternating

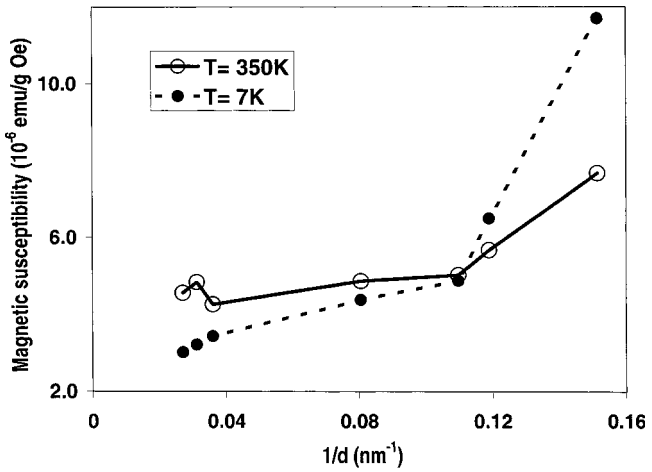


FIG. 8. Plot of magnetic susceptibility $\chi$ at the temperatures of 7 and 350 K vs $1/d$, where $d$ is the particle size in nm. Lines joining the points are for visual aid.

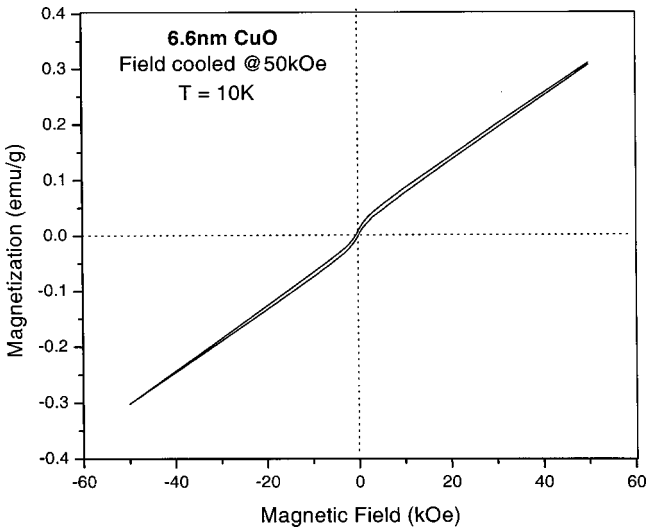


FIG. 9. Hysteresis loop at 10 K for the 6.6-nm particles for the FC case in $H=50$ kOe.

planes belonging to the same sublattice on the surface layer are uncompensated. For the 6.6-nm particles, measurements of the hysteresis loop parameters clearly show a magnetic transition below 40 K and anomalous hysteresis loops up to 330 K. These results are presented next.

### E. Hysteresis loops

We have carried out detailed hysteresis loop measurements for the 6.6-nm particles as a function of temperature to 330 K for both the ZFC and FC cases. In Figs. 9 and 10, we show the measured hysteresis loops in which $M_r$ (remanence) is the average of the positive and negative intercepts on the $M$ axis and $H_c$ (coercivity) is the half width of the loop at $H=0$. The hysteresis loops are narrow (with $H_c<300$ Oe) yet open even at 50 kOe. For ZFC, the temperature variation of $H_c$ and $M_r$ is plotted in Fig. 11. There is a dramatic increase in both $M_r$ and $H_c$ below 40 K, mirroring

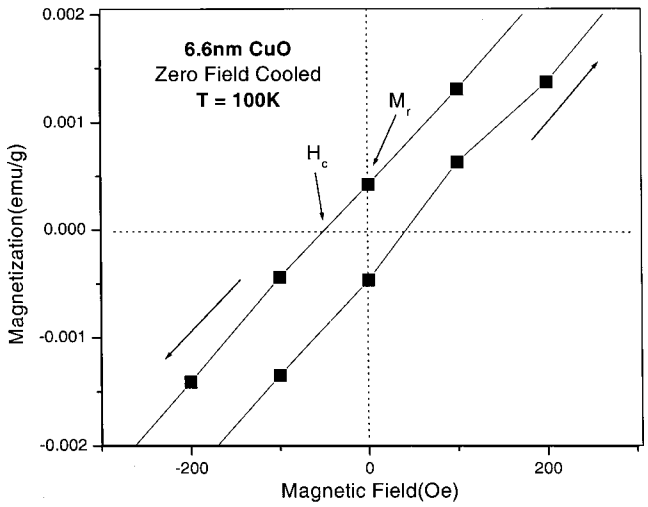


FIG. 10. Details of the hysteresis loop for the 6.6-nm particles in the low-field region at 100 K.

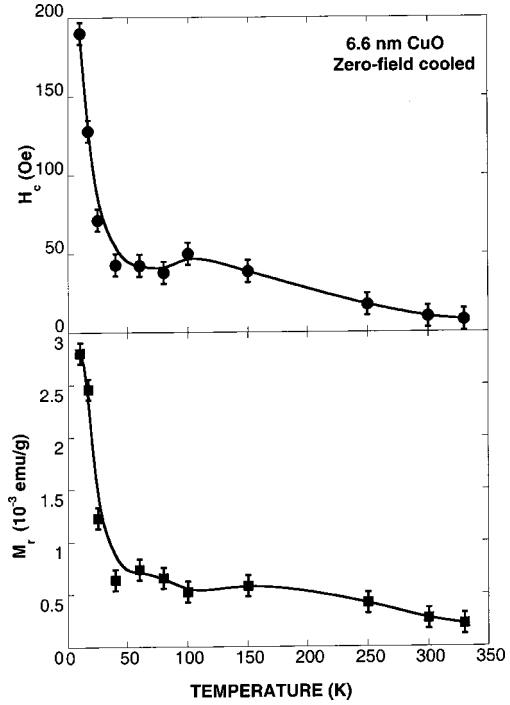


FIG. 11. Temperature variations of the coercivity $H_c$ and remanence $M_r$ for the zero-field cooled case. Lines through the data points are for visual aid. Error bars represent experimental uncertainties.

the increase in $\chi$ observed in Fig. 4 below 40 K. Above 40 K, both $H_c$ and $M_r$ decrease slowly with an increase in temperature, so that at room temperature $H_c \simeq 10$ Oe is observed. The most interesting aspect of these observations is the transition at 40 K and the observation of a hysteresis loop at room temperature (well above the expected $T_N \leqslant 170$ K as noted earlier).

To gain further insight into the nature of transition at 40 K, we measured hysteresis loops under FC conditions using $H = 50$ kOe. The data for the low-field region (Fig. 12) show not only a shift $H_E$ of the hysteresis loop to negative direction expected from exchange bias,[29] but also broadening of the loop (increase in $H_c$). The temperature variations of $H_c$

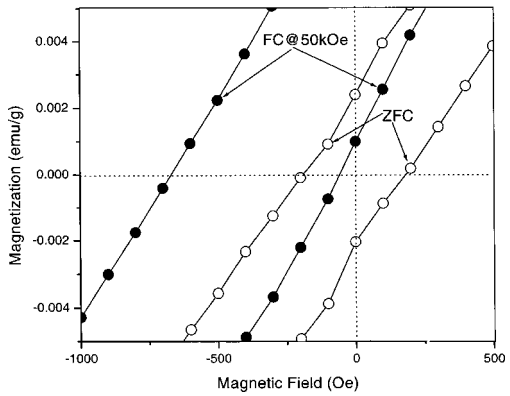


FIG. 12. Comparison of the hysteresis loop for the 6.6-nm particles under the field-cooled and zero-field-cooled conditions. Under FC, the loop is shifted and broadened.

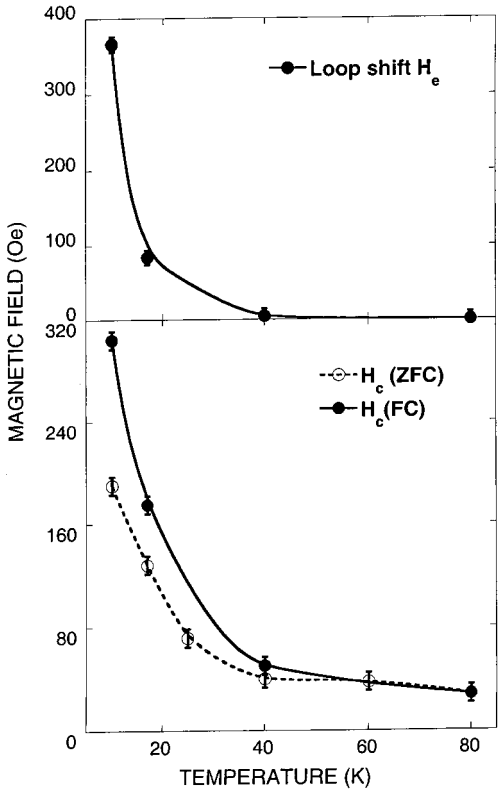


FIG. 13. Plot of the temperature variation of the coercivity $H_c$ and loop shift $H_E$ for the FC 6.6-nm particles in $H = 50$ kOe. Data of $H_c$ for the zero-field cooled case are also shown for comparison. Lines through the data points are for visual aid. Error bars represent experimental uncertainties.

and $H_E$ (Fig. 13) show that above 40 K, $H_E$ is zero and $H_c$ values become equal to those observed for ZFC (Fig. 11). So the main conclusions from these investigations is that $T = 40$ K represents a transition to a magnetic state for which exchange bias is present.

### F. Transition at 40 K

What is a plausible explanation for the presence of a hysteresis loop but the absence of exchange anisotropy or bias above $T \simeq 40$ K? This temperature is not $T_B$, the blocking temperature, because for $T > T_B$, no hysteresis should be present, whereas in our case, hysteresis is observed up to 330 K. Also, the temperature dependence of $\chi$ above 40 K in the 6.6-nm particles does not follow the behavior expected for a superparamagnet above $T_B$. Instead, these results for the 6.6-nm CuO nanoparticles are qualitatively similar to the reported observations in the Permalloy/CoO system.[30] Here Permalloy ($Ni_{80}Fe_{20}$) has ferromagnetic ordering with $T_c \simeq 800$ K, whereas CoO orders antiferromagnetically with $T_N \simeq 291$ K. As the system is cooled through $T_N$ of CoO in a magnetic field, the ferromagnetically ordered Permalloy displays a uniaxial anisotropy manifested in the loop shift $H_E$. In this case $H_E$ disappears above $T_N \simeq 291$ K, although $H_c$ remains nonzero above $T_N$ with a temperature dependence very similar to our observation in CuO shown in Fig. 13.

Therefore, it is likely that in the 6.6-nm CuO particles, $T_N = 40\,\mathrm{K}$ represents the Néel temperature of $Cu^{2+}$ spins in the core, whereas the ferromagnet component is provided by the uncompensated surface spins on the same sublattice as discussed earlier. Because of the large exchange interaction [$J \simeq 400\,\mathrm{K}$ (Ref. 19)] between $Cu^{2+}$ ions, this short-range ferromagnetic ordering between the uncompensated surface spins in the same sublattice and the short-range ordering of the spins in the core extends to well above 330 K. Our observation of a weak-ferromagnetic component even at 330 K (Fig. 7) supports this view. Of course, the strong exchange coupling between the uncompensated surface spins and the spins in the core is responsible for the observed exchange anisotropy, which disappears when antiferromagnetic ordering in the core is lost above $T_N \simeq 40\,\mathrm{K}$.

### G. Concluding remarks

Recently, Kodama and Berkowitz[3] have reported their results on the atomic-scale modeling of the magnetic properties of the nanoparticles of $NiFe_2O_4$, $\gamma$-$Fe_2O_3$, and NiO. According to these results, the high-field irreversibility of magnetization may be attributed to the canting of the surface spins, with lower coordination and broken exchange bonds. These surface spins, with multiple spin configurations, freeze into a spin-glass state below $T_B$, leading to $H_E$ and large $H_c$ for $T < T_B$. Further, magnetic order for the core spins can be quite different from that observed in bulk systems because the disorder of the surface spins in nanoparticles is communicated to the core spins via exchange coupling. Although some of the conclusions from these studies[3] may also be valid for CuO NP's, care needs to be exercised since the crystal and magnetic structures, and exchange parameters for CuO are quite different. Our observation of hysteresis loops in the 6.6-nm CuO up to 330 K, well above $T_N \simeq 40\,\mathrm{K}$, is quite unique. It is hoped that these new results in CuO will provide the impetus for atomic-scale modeling of the magnetic structure of this system.

In summary, the results presented here have shown that CuO NP's below 10 nm exhibit nanoparticle magnetism with uncompensated surface spins resulting in a weak-ferromagnetic component. For the 6.6-nm particles, $T_N \simeq 40\,\mathrm{K}$ for the spins in the core is inferred. Below this $T_N$, exchange bias and enhanced coercivities are observed. The observation of hysteresis loops up to 330 K suggests weakly aligned uncompensated spins due to short-range order present as a result of a large exchange interaction. For particles greater than 10 nm, the magnetic ordering is essentially similar to the antiferromagnetic ordering of the bulk CuO, but with a reduced $T_N$ because of the expansion of the lattice.

### ACKNOWLEDGMENTS

This research was supported in part by the U.S. Department of Energy, Contract No. DE-FC26-99FT40540. We thank Dr. S. Chu for experimental assistance, and Carnegie Mellon University, where some of the magnetic measurements were carried out. Identification of commerical equipment in the text does not imply recommendation or endorsement by the authors or their employers.

*Corresponding author. Electronic address: mseehra@wvu.edu

[1] See various papers in *Magnetic Properties of Fine Particles*, edited by J. L. Dormann and D. Fiorani (Elsevier Science, Amsterdam, 1992); *Nanophase Materials: Synthesis, Properties, Applications*, edited by G. C. Hadjipanayis and R. W. Siegel (Kluwer, Dordrecht, 1994).

[2] D. E. Speliotis, J. Magn. Magn. Mater. **193**, 29 (1999).

[3] R. H. Kodama and A. E. Berkowitz, Phys. Rev. B **59**, 6321 (1999).

[4] L. Néel, in *Low Temperature Physics*, edited by C. Dewitt, B. Dreyfus, and P. G. de Gennes (Gordon and Breach, New York, 1962), p. 413.

[5] S. A. Makhlouf, F. T. Parker, and A. E. Berkowitz, Phys. Rev. B **55**, R14 717 (1997).

[6] S. A. Makhlouf, F. T. Parker, F. E. Spada, and A. E. Berkowitz, J. Appl. Phys. **81**, 5561 (1997).

[7] M. S. Seehra, V. S. Babu, A. Manivannan, and J. W. Lynn, Phys. Rev. B **61**, 3513 (2000).

[8] S. Gider, D. D. Awschalom, T. Douglas, S. Mann, and M. Chaparala, Science **268**, 77 (1995).

[9] R. Zysler, D. Fiorani, J. L. Dormann, and A. M. Testa, J. Magn. Magn. Mater. **13**, 71 (1994).

[10] M. M. Ibrahim, J. Zhao, and M. S. Seehra, J. Mater. Res. **7**, 1856 (1992).

[11] J. L. Jambor and J. E. Dutrizac, Chem. Rev. **98**, 2549 (1998).

[12] S. Asbrink and L.-J. Norrby, Acta Crystallogr., Sect. B: Struct. Crystallogr. Cryst. Chem. **26**, 8 (1970).

[13] M. O'Keeffe and F. S. Stone, J. Phys. Chem. Solids **23**, 261 (1962).

[14] M. S. Seehra, Z. Feng, and R. Gopalakrishnan, J. Phys. C **21**, 1051 (1988).

[15] D. D. Lawrie, J. P. Frank, and C-T. Lin, Physica C **297**, 59 (1998).

[16] J. W. Loram, K. A. Mirza, C. P. Joysce, and A. J. Osborne, Europhys. Lett. **8**, 263 (1989).

[17] S. B. Ota and E. Gmelin, Phys. Rev. B **46**, 11 632 (1992).

[18] J. B. Forsyth, P. J. Brown, and B. M. Wanklyn, J. Phys. C **21**, 2917 (1988); M. Ain, A. Menelle, B. M. Wanklyn, and E. F. Bertaut, J. Phys.: Condens. Matter **4**, 5327 (1992); B. X. Yang, T. R. Thurston, J. M. Tranquada, and G. Shirane, Phys. Rev. B **39**, 4343 (1989).

[19] O. Kondo, M. Ono, E. Sugiura, K. Sugiyama, and M. Date, J. Phys. Soc. Jpn. **57**, 3293 (1988); K. Kindo, M. Honda, T. Kohashi, and M. Date, *ibid.* **59**, 2332 (1990).

[20] T. V. C. Rao and V. C. Sahni, J. Phys.: Condens. Matter **6**, L423 (1994).

[21] J. Kobler and T. Chattopadhay, Z. Phys. B: Condens. Matter **82**, 383 (1991).

[22] K. Borgohain, J. B. Singh, M. V. Rama Rao, T. Sripathi, and S. Mahamuni, Phys. Rev. B **61**, 11 093 (2000).

[23] V. R. Palkar, P. Ayyub, S. Chattopadhay, and M. Multani, Phys. Rev. B **53**, 2167 (1996).

[24] P. Ayyub, V. R. Palkar, S. Chattopadhay, and M. Multani, Phys. Rev. B **51**, 6135 (1995).

[25] For ZFC, after cooling the sample to 5 K in $H = 0$, $M$ is measured

with increasing $T$ in $H=200$ Oe. For FC, the data are taken with decreasing $T$ starting from 350 K.

[26] M. E. Fisher, Philos. Mag. **7**, 1731 (1962); E. E. Bragg and M. S. Seehra, Phys. Rev. B **7**, 4197 (1973).

[27] D. Bloch, J. Phys. Chem. Solids **27**, 881 (1966): The experimental results in this reference yield $\gamma_m = -\partial \ln T_N / \partial \ln R \simeq 10$, where $R$ is the distance between magnetic ions assuming $T_N \propto J$. The larger magnitude of $\gamma_m$ observed here in CuO may reflect contributions from the finite-size effects which usually begin to become important below about 10 nm; see, e.g., P. Poulopoulos and K. Baberschke, J. Phys.: Condens. Matter **11**, 9495 (1999).

[28] J. T. Richardson, D. L. Yiagas, B. Turk, K. Forster, and M. V. Twigg, J. Appl. Phys. **70**, 6977 (1991).

[29] See the reviews by A. E. Berkowitz and K. Takano, J. Magn. Magn. Mater. **200**, 552 (1999); J. Nogues and I. K. Schuller, *ibid.* **192**, 203 (1999).

[30] T. J. Moran, J. M. Gallego, and I. K. Schuller, J. Appl. Phys. **78**, 1887 (1995).